Controlled preparation of $CoNi_2S_4$ nanorods derived from MOF-74 nanoarrays involving exchange reaction for high energy density supercapacitors

Qihang Chen,[a] Wenna Zhao,[b,*] Zihao Huang,[a] Guochang Li, [a] Kai Tao[a] and Lei Han [a,*]

[a] School of Materials Science & Chemical Engineering, Ningbo University, Ningbo, Zhejiang 315211, China

[b] School of Biological and Chemical Engineering, Ningbotech University, Ningbo, Zhejiang 315100, China

* Corresponding authors.

E-mail addresses: wnzhao@nit.zju.edu.cn (W. Zhao); hanlei@nbu.edu.cn (L. Han)

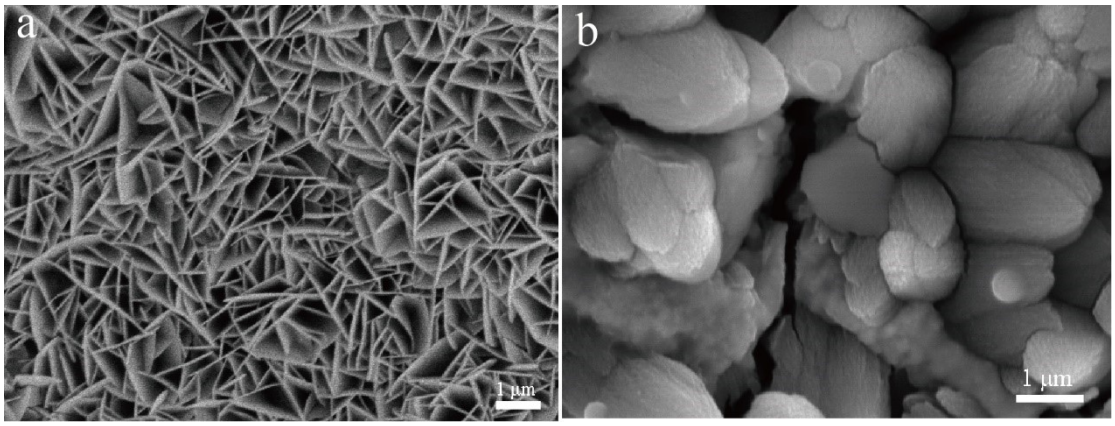

Fig. S1. SEM image of (a) NiCo-LDH, (b) NiCo-MOF-74 direct sulfidation (NiCo-S).

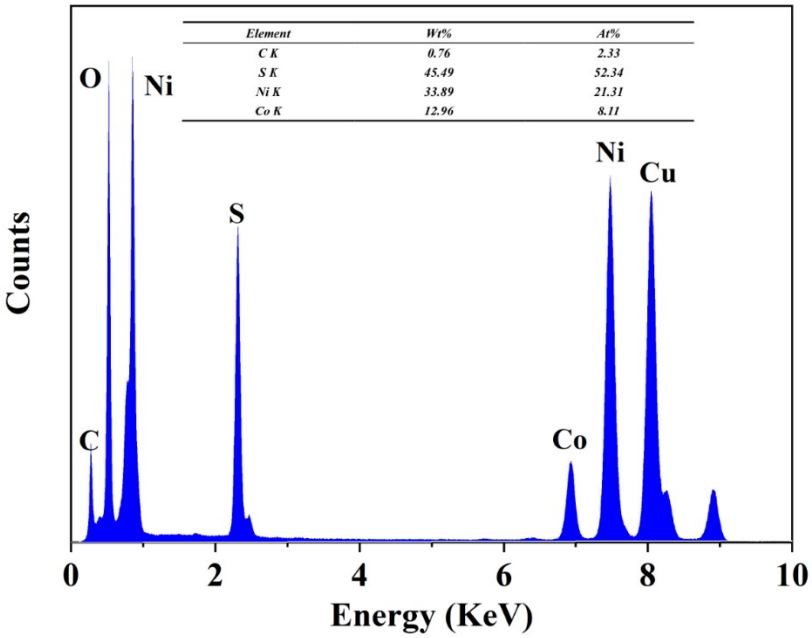

Fig. S2. The EDS spectrum of $CoNi_2S_4$ scraped from Ni foam.

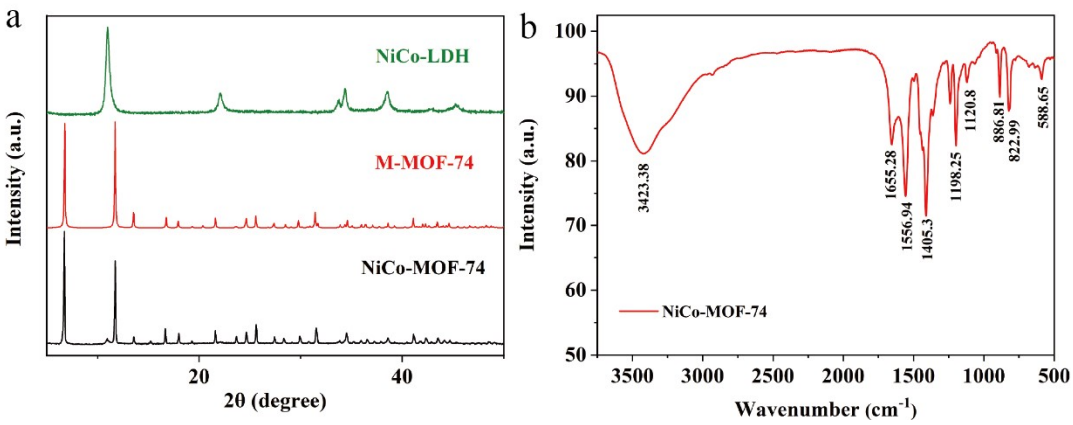

Fig. S3. (a) XRD patterns of NiCo-MOF-74 and NiCo-LDH, (b) FT-IR spectra of NiCo-MOF-74.

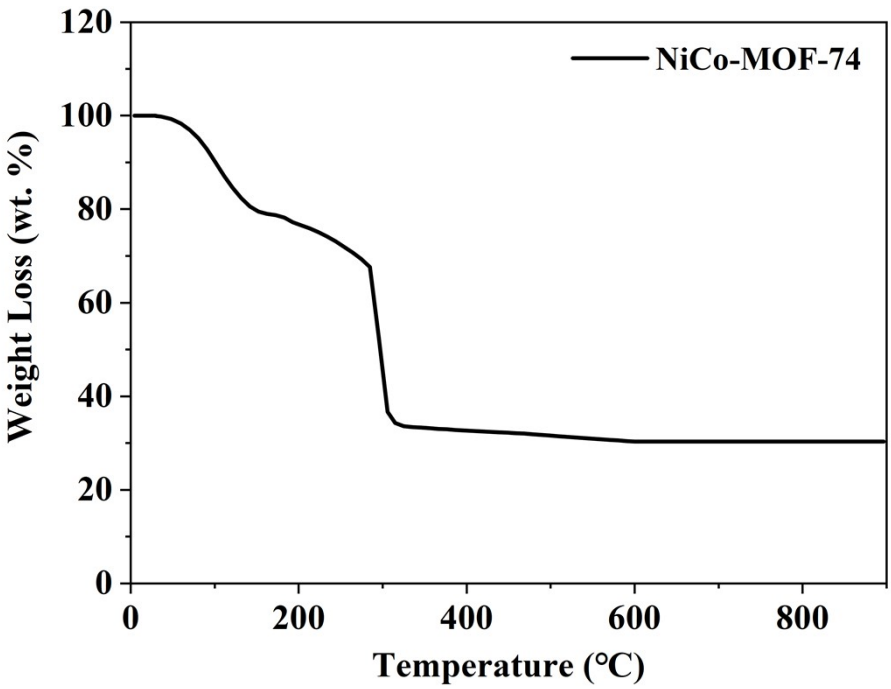

Fig. S4. TGA curves of NiCo-MOF-74.

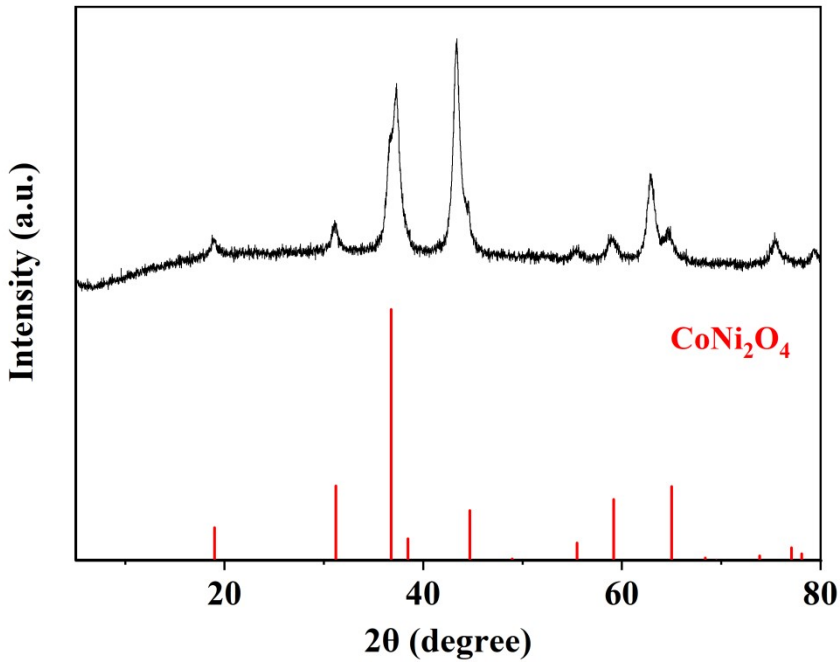

Fig. S5. XRD patterns of $CoNi_2O_4$.

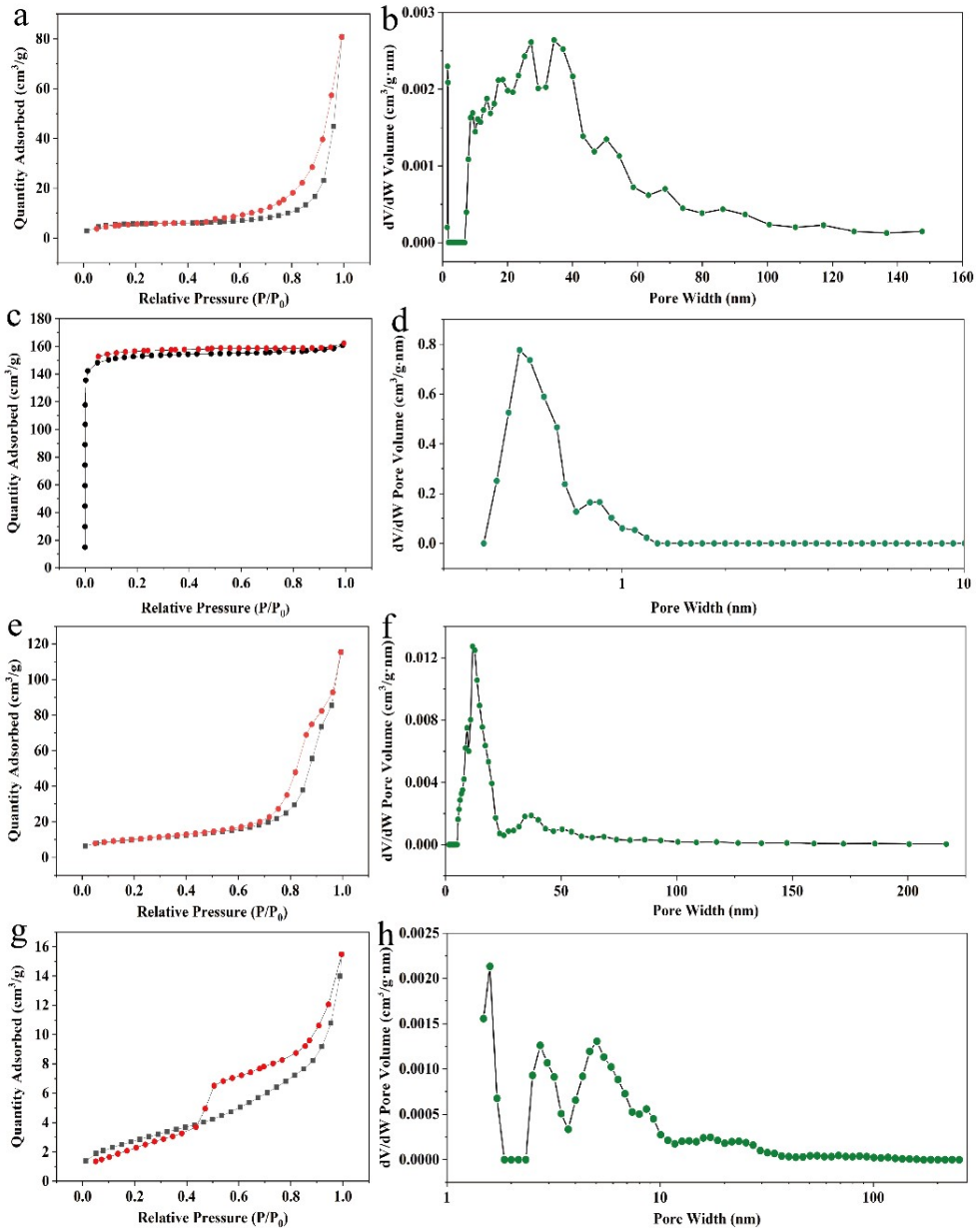

Fig. S6. N_2 adsorption-desorption isotherms curves of (a) NiCo-LDH, (c) NiCo-MOF-74, (e) $CoNi_2O_4$, (g) $CoNi_2S_4$; pore-size distribution curves of (b) NiCo-LDH, (d) NiCo-MOF-74, (f) $CoNi_2O_4$, (h) $CoNi_2S_4$.

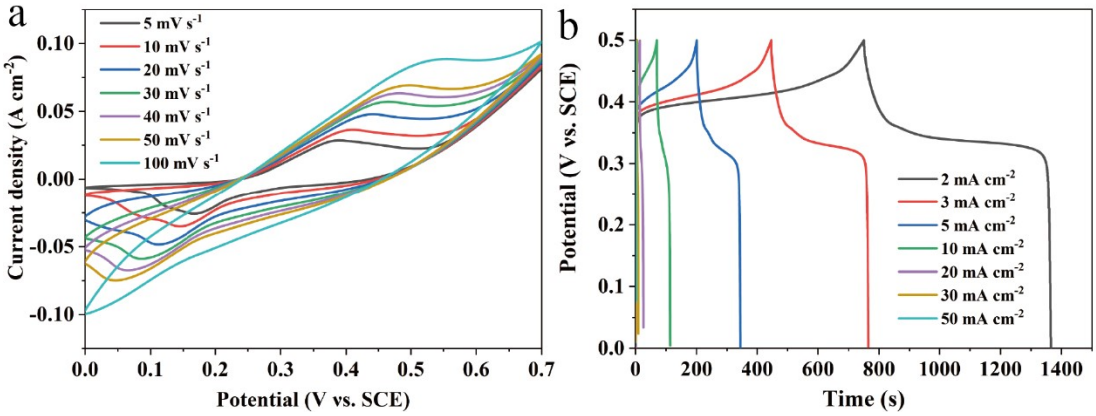

Fig. S7. (a) CV curves of NiCo-LDH at different scan rates, (b) GCD curves of NiCo-LDH at different current densities.

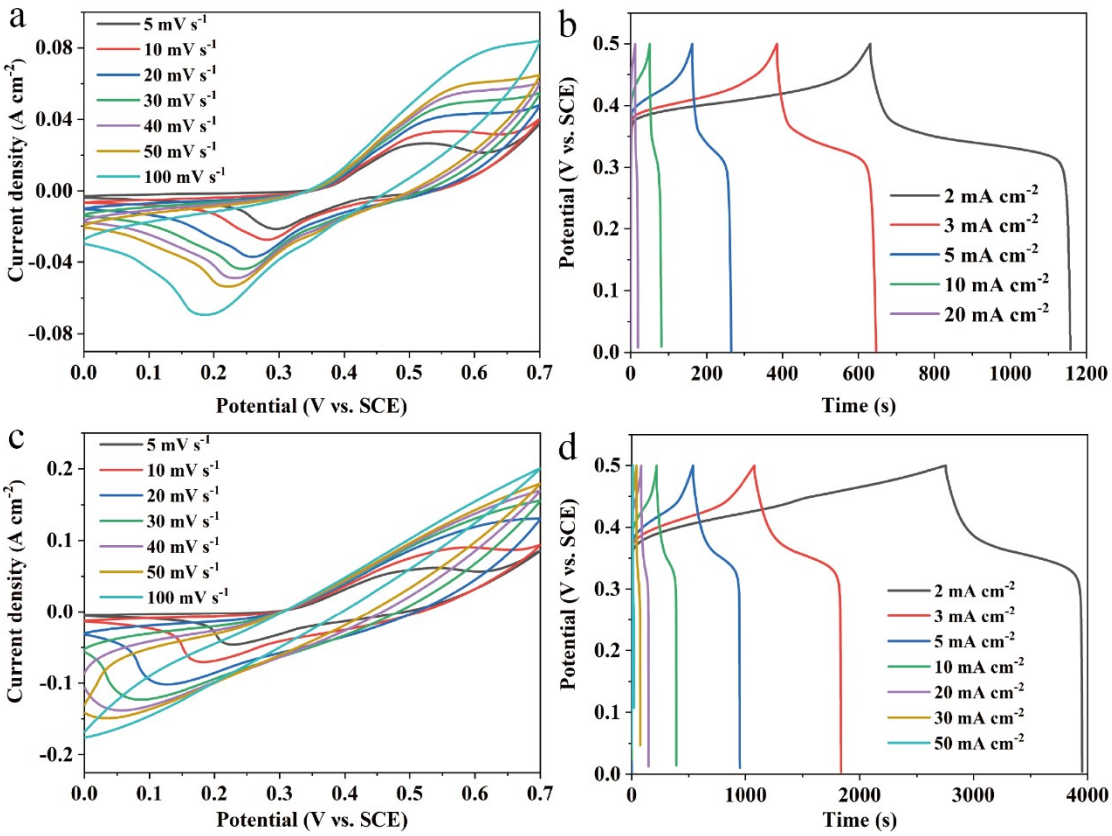

Fig. S8. (a) CV curves of $CoNi_2O_4$ at different scan rates, (b) GCD curves of $CoNi_2O_4$ at different current densities, (c) CV curves of NiCo-MOF-74 at different scan rates, (d) GCD curves of NiCo-MOF-74 at different current densities.

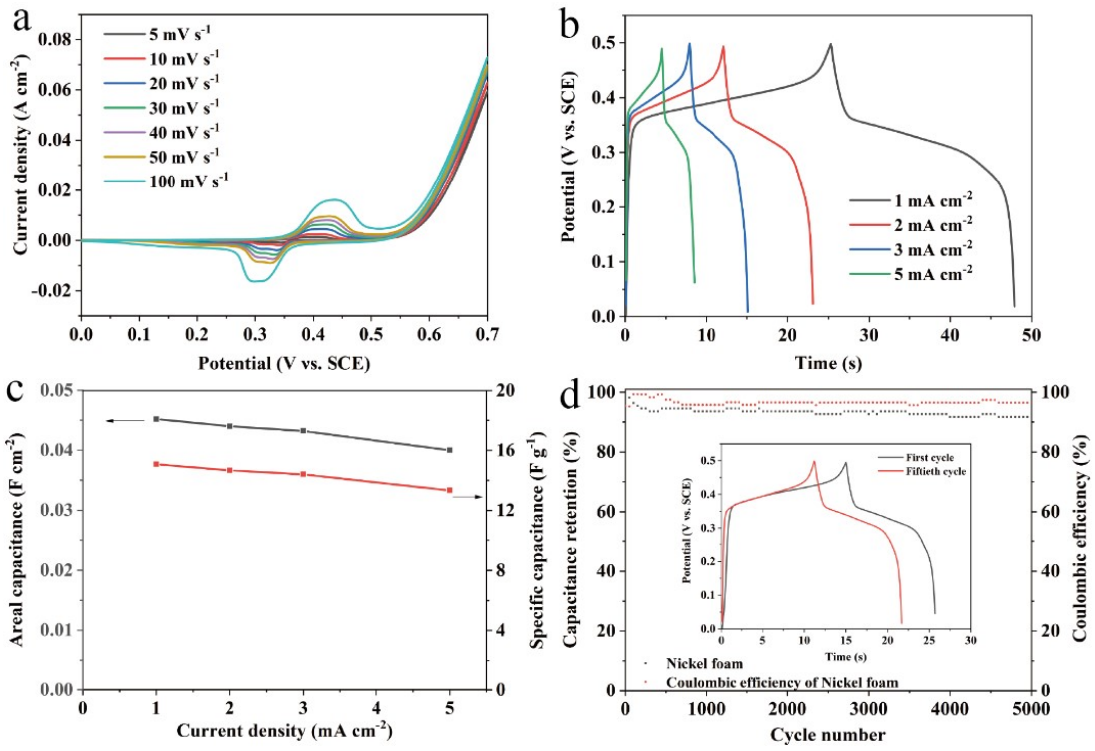

Fig. S9. (a) CV curves of Ni-foam at different scan rates, (b) GCD curves of Ni-foam at different current densities, (c) areal/specific capacitances of Ni-foam, (d) cycling performances and Coulomb efficiency of Ni-foam.

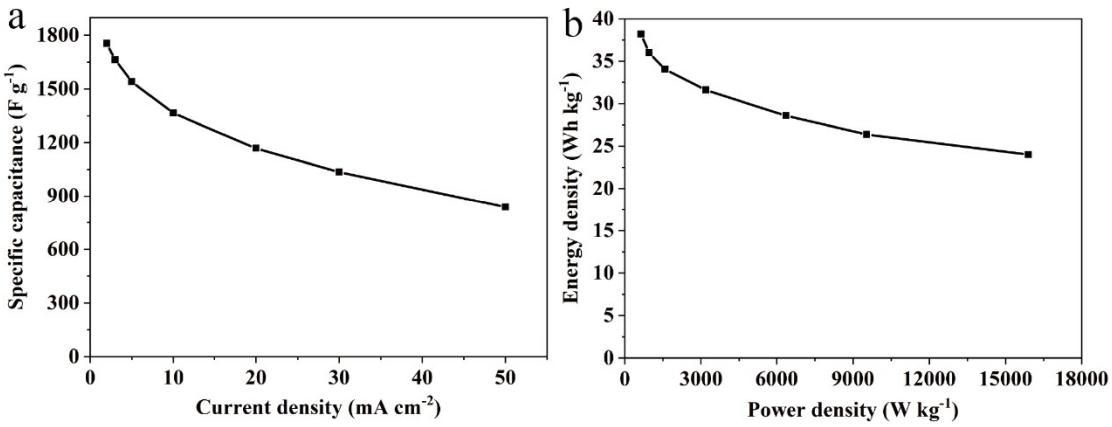

Fig. S10. (a) specific capacitances of $CoNi_2S_4$, (b) Energy and power densities of $CoNi_2S_4$.

Table. S1. EIS parameters of electrodes with different electrodes.

Electrodes	R_s	R_{ct}
$CoNi_2S_4$	0.43 Ω	0.08 Ω
$CoNi_2O_4$	1.53 Ω	0.20 Ω
NiCo-MOF-74	1.18 Ω	0.95 Ω
NiCo-LDH	1.53 Ω	0.09 Ω

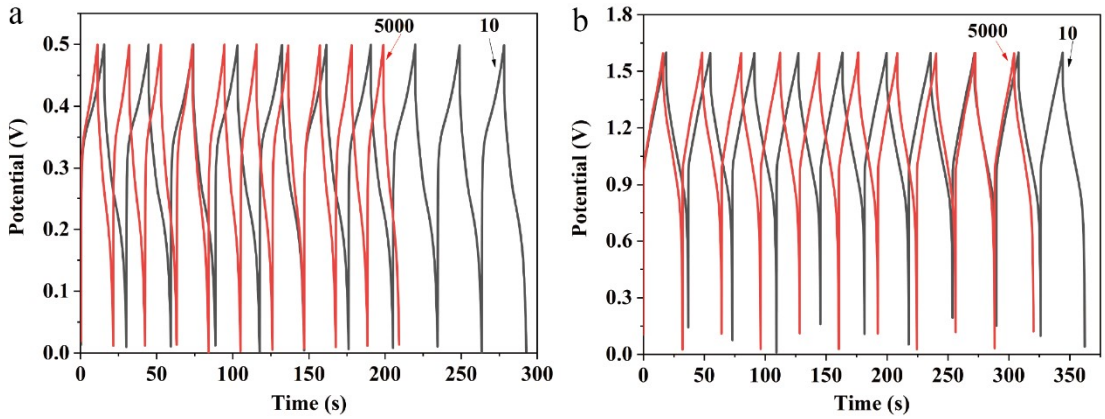

Fig. S11. (a) Cycling performance of $CoNi_2S_4$, (b) Cycling performance of ACS device.

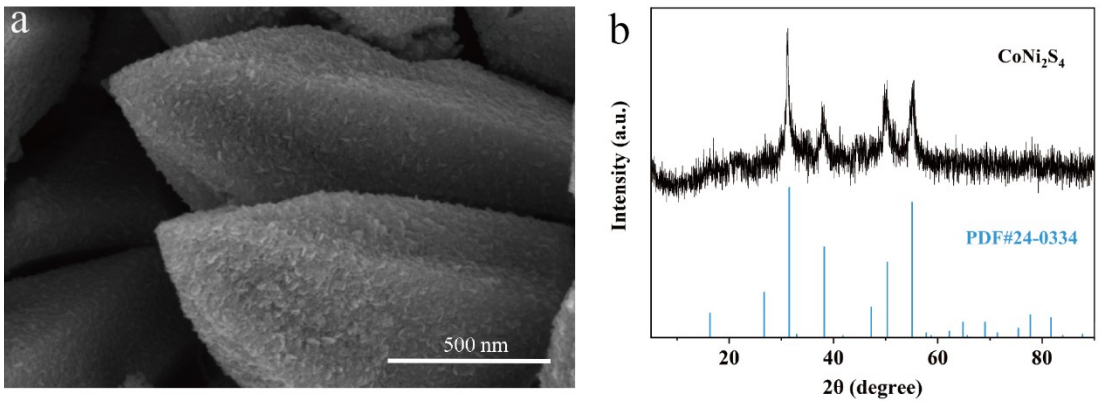

Fig. S12. (a) SEM, (b) XRD patterns of $CoNi_2S_4$ after cycling test.

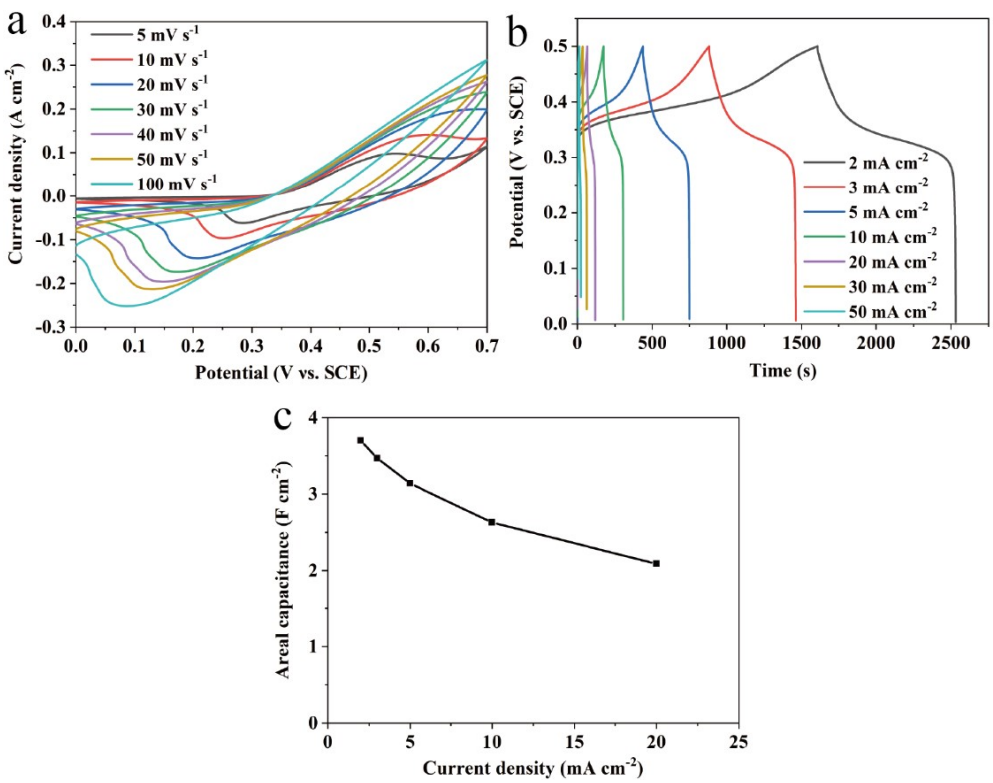

Fig. S13. (a) CV curves; (b) GCD curves; (c) areal capacitances of NiCo-MOF-74 grown directly on nickel foam.

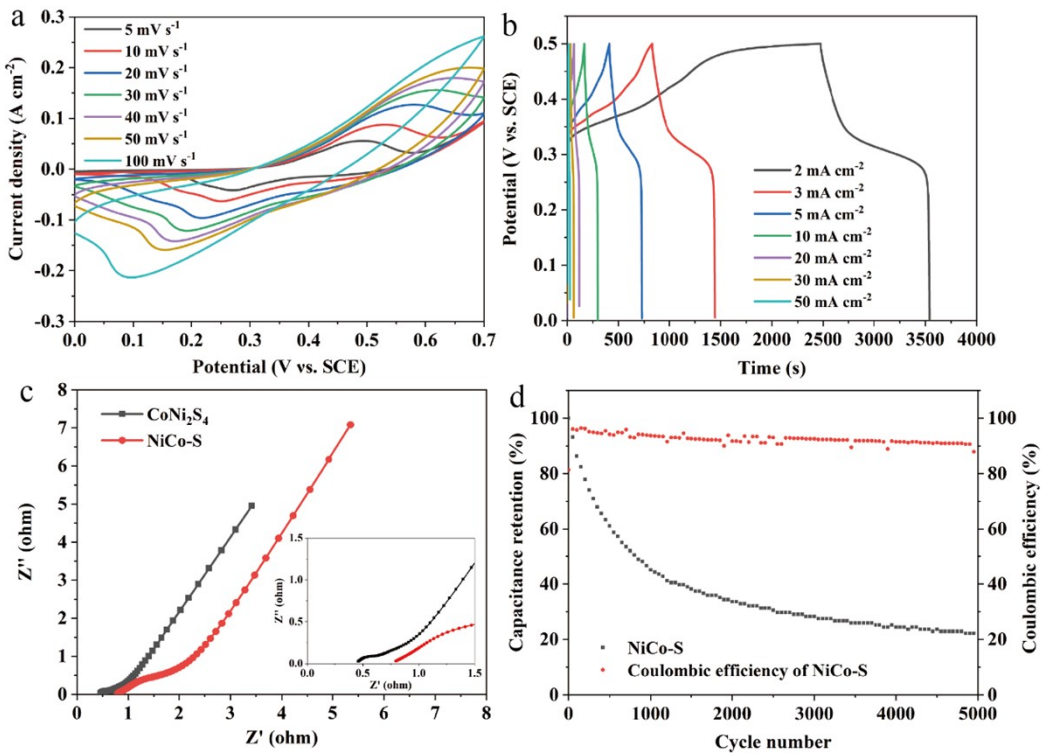

Fig. S14. (a) CV curves of NiCo-S at different scan rates, (b) GCD curves of NiCo-S at different current densities, (c) EIS spectra of NiCo-S and $CoNi_2S_4$, (d) cycling performances and Coulomb efficiency of NiCo-S.

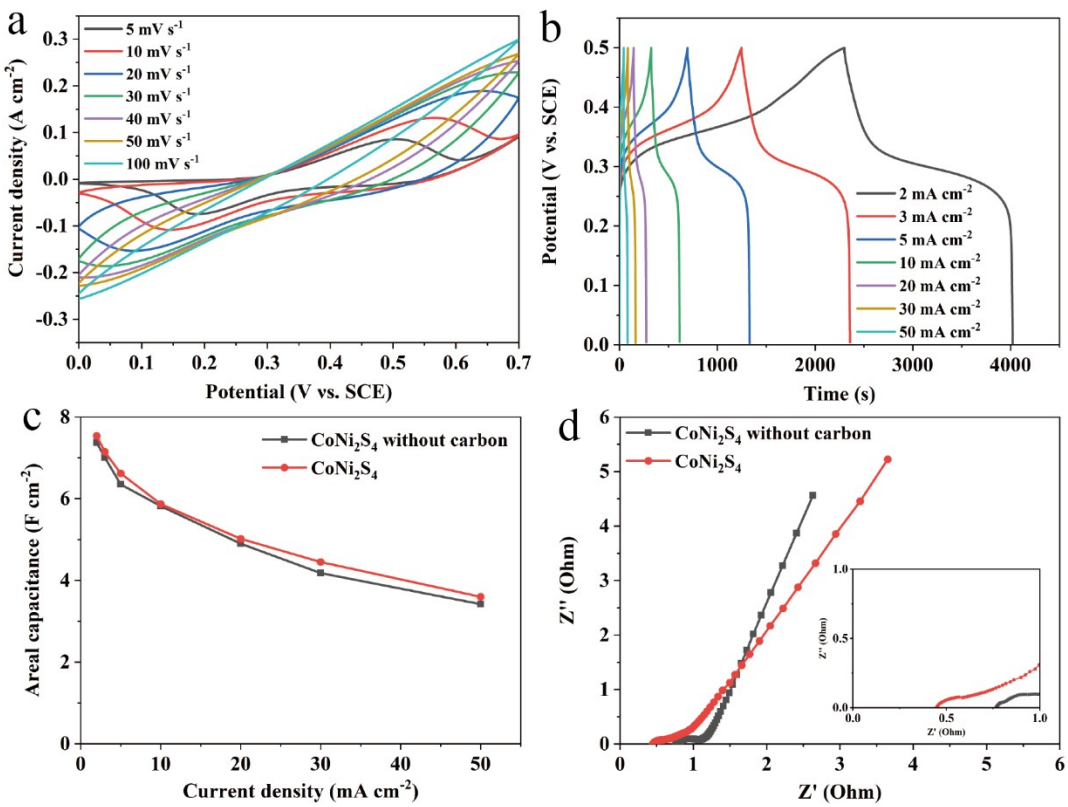

Fig. S15. (a) CV curves; (b) GCD curves; (c) areal capacitances, (d) EIS spectra of $CoNi_2S_4$ without carbon.

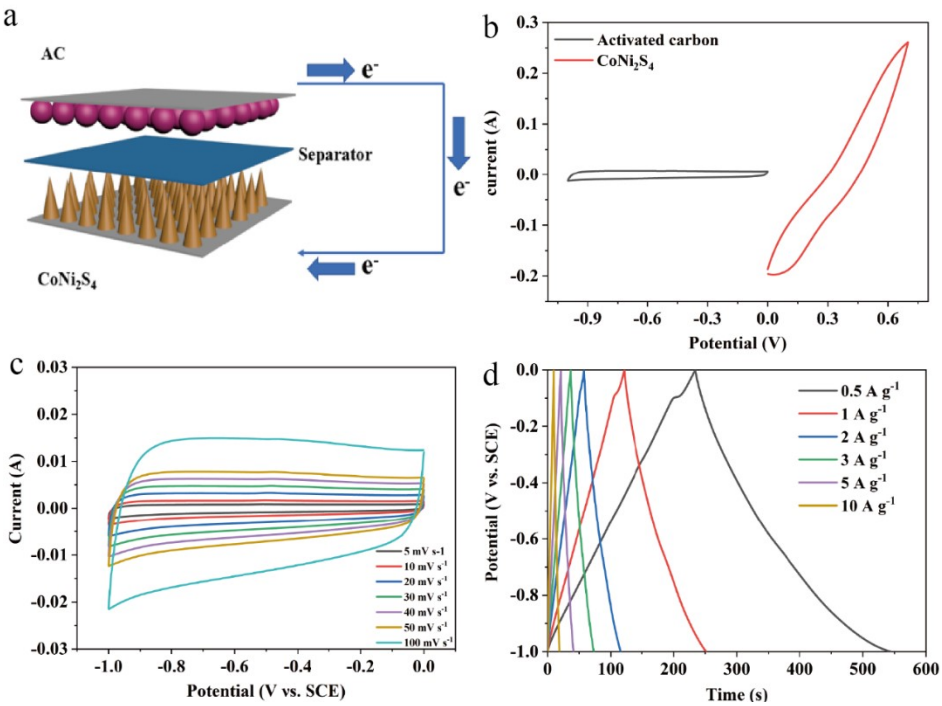

Fig. S16. (a) Schematic illustration of ASC, (b) CV curves of AC and $CoNi_2S_4$ at a scan rate of 50 mV s^{-1}, (c) CV curves of AC at different scan rates, (d) GCD curves of AC at different current densities.

Fig. S17. Two series-connected ASC devices light up the LEDs.